Journal of Medicinal Chemistry Article

J. Med. Chem. **2011,** *54,* 143–152 **143**
DOI: 10.1021/jm100966t

Gd-Complexes of 1,4,7,10-Tetraazacyclododecane-*N*,*N*′,*N*″,*N*‴-1,4,7,10-tetraacetic Acid (DOTA) Conjugates of Tranexamates as a New Class of Blood-Pool Magnetic Resonance Imaging Contrast Agents

Sungwook Gu,[†,⊥] Hee-Kyung Kim,[‡,⊥] Gang Ho Lee,[§] Bong-Seok Kang,[∥] Yongmin Chang,*[,‡,#] and Tae-Jeong Kim*[,†]

[†]*Department of Applied Chemistry,* [‡]*Department of Medical and Biological Engineering,* [§]*Department of Chemistry, and* [∥]*Bio-Medical Research Institute,* [#]*Department of Diagnostic Radiology & Molecular Medicine, Kyungpook National University, 1370 Sankyuk-dong, Buk-gu, Daegu 702-701, Republic of Korea.* [⊥]*These authors contributed equally.*

Received July 29, 2010

Gd-complexes of the type $[Gd(L)(H_2O)]\cdot xH_2O$ (**5a**−**c**), where L is DOTA conjugates of tranexamic acid (**4a**) and tranexamic esters (**4b**,**c**), have been prepared as a new class of MRI blood-pool contrast agents (BPCAs). Thermodynamic stability (K_{GdL}) and pharmacokinetic inertness of **5** compare well with or better than those of analogous MRI contrasting agents (CAs) such as Gd-DOTA and Gd-DTPA-BMA. Their R_1-relaxivities are significantly higher than those of any of the clinically used MRI CAs. T_1-weighted MR images of mice administered by **5c** demonstrate high blood-pool effect with simultaneous contrast enhancement in liver. The structural uniqueness of **5c** lies in the fact that it adopts macrocyclic DOTA instead of acyclic DTPA. In addition, **5c** is nonionic and makes no resort to aromatic substituent(s) in the chelate backbone for the blood-pool enhancement. The nature of hepatobiliary uptake demonstrated by **5c** may be explained in terms of lipophilicity of tranexamate in the chelate (**4c**). The cell cytotoxicity test shows no toxicity found with **5**, suggesting their use as a practical MRI BPCAs.

Introduction

Over the past 3 decades, magnetic resonance imaging (MRI[a]) has been one of the most powerful techniques for the noninvasive diagnostic technique of the human anatomy, physiology, and pathophysiology on the basis of superior spatial resolution and contrast.[1] In general, contrast agents (CAs) are employed in MRI to improve the contrast effect, and Gd(III), with its high magnetic moment and long electron spin relaxation time, is an ideal candidate for such a proton relaxation agent and is the most famous metal center for contrast enhancement.[2] To date, more than 200 million patients have been exposed to gadolinium based contrast agents (GBCAs) in the world.[3]

There are now known various types of GBCAs currently employed for clinical uses and may be classified into several groups according to their structural features as well as the charge of the complex.[4−7] As a whole, four types of Gd-chelate may be recognized. They are (1) anionic Gd-(acyclic chelates) such as $[Gd(DTPA)(H_2O)]^{2-}$ (DTPA = diethylentriamine-*N*,*N*,*N*′,*N*″,*N*″-pentaacetic acid), (2) neutral Gd-(acyclic chelates) such as [Gd(DTPA-BMA)(H_2O)] (DTPA-BMA = *N*,*N*″-bis(methylamide) of DTPA), (3) anionic Gd-(cyclic chelates) such as $[Gd(DOTA)(H_2O)]^{1-}$ (DOTA = 1,4,7,10-tetraazacyclododecane-*N*,*N*′,*N*″,*N*‴-1,4,7,10-tetraacetic acid), and (4) neutral Gd-(cyclic chelates) such as [Gd-(HP-DO3A)(H_2O)] (HP-DO3A = 10-(2-hydroxypropyl)-1,4,7,10-tetraazacyclododecane-*N*,*N*′,*N*″,*N*‴-1,4,7-triacetic acid).

Each type of these MRI CAs possesses its own merits and drawbacks. For instance, a neutral type is preferred over an anionic one in that the former exhibits relatively low osmotic pressure in the body fluids after intravenous administration.[2,8] As for the thermodynamic stability and kinetic inertness of CAs, a macrocyclic chelate such as DOTA or DO3A might be preferred over an acyclic, open-chain counterpart such as DTPA of DTPA-bis(amide). All these MRI CAs listed above have a common feature in that they are extracellular fluid (ECF) agents. Therefore, despite their successful applications, they have some inherent drawbacks such as poor contrast enhancement due to low R_1-relaxivity, nonspecificity, and rapid renal excretion. There thus arises the need for new MRI CAs with improved performances and at the same time with special functionality. Much effort has recently been made to develop new classes of MRI CAs for use as (1) organ or tumor targeting MRI CAs, (2) blood-pool MRI CAs, and (3) smart MRI CAs.[9−12]

*To whom correspondence should be addressed. For Y.C.: phone, (+)82-53-420-5471; fax, (+)82-53-421-4974; e-mail, ychang@knu.ac.kr. For T.-J.K.: phone, (+)82-53-950-5587; fax, (+)82-53-950-6594; e-mail, tjkim@knu.ac.kr.

[a] Abbreviations: BOPTA, 4-carboxy-5,8,11-tris(carboxylmethyl)-1-phenyl-2-oxa-5,8,11-triazatridecan-13-oic acid; CAs, contrast agents; BPCA, blood-pool contrast agents; CNR, contrast to noise ratio; DO3A, 1,4,7,10-tetraazacyclododecane-*N*,*N*′,*N*″-1,4,7-triacetic acid; DOTA, 1,4,7,10-tetraazacyclododecane-*N*,*N*′,*N*″,*N*‴-1,4,7,10-tetraacetic acid; DTPA, diethylentriamine-*N*,*N*,*N*′,*N*″,*N*″-pentaacetic acid; DTPA-BMA, *N*,*N*″-bis(methylamide) of diethylentriamine-*N*,*N*,*N*′,*N*″,*N*″-pentaacetic acid; ECF, extracelluar fluid; EOB-DTPA, *S*-[4-(4-ethoxybenzyl)-3,6,9-tris(carboxylatomethyl)-3,6,9-triazaundecanedioic acid; FOV, field of view; GBCAs, gadolinium based contrast agents; HP-DO3A, 10-(2-hydroxypropyl)-1,4,7,10-tetraazacyclododecane-*N*,*N*′,*N*″,*N*‴-1,4,7-triacetic acid; ICR, Institute of Cancer Research; MRI, magnetic resonance imaging; NEX, number of acquisition; ROI, regions of interest; TE, echo time; TFA, trifluoroacetic acid; TI, inversion time; TMS, tetramethylsilane; TR, repetition time.

Published on Web 12/09/2010

The purpose of the present work is to design and synthesize some new MRI BPCAs with improved R_1-relaxivity and thermodynamic stability as well as kinetic inertness. Our initial approach is to design a series of DOTA conjugates of tranexamic acid and its esters. The choice of tranexamic entity is based on our early observations that the chelates incorporating this particular molecular entity help, most of all, to increase the R_1-relaxivities of resulting Gd-chelates such as **6** (Chart 1) (up to 3 times as high as that of Gd-DTPA-BMA) by way of increasing rotational correlation time (τ_R)[13] and at the same time make it possible to control relaxivity by varying the substituent of the carboxylic moiety (−COOR).[14,15] It has also been observed that the tranexamic group adds lipophilicity to the Gd-complex, a prerequisite for better interaction with organs such as liver. In this connection, both Gd-BOPTA (BOPTA = 4-carboxy-5,8,11-tris(carboxylmethyl)-1-phenyl-2-oxa-5,8,11-triazatridecan-13-oic acid) and Gd-EOB-DTPA (EOB-DTPA = *S*-[4-(4-ethoxybenzyl)-3,6,9-tris(carboxylatomethyl)-3,6,9-triazaundecanedioic acid), two representative liver specific MRI CAs currently available in the market, adopt the acyclic DTPA moiety whose backbone is derivatized by an aromatic residue for better hepatocellular uptake and biliary excretion.[16−18] Finally, further justification for the selection of tranexamic derivatives in this work comes from the fact that they have been used as antifibrinolytic drugs with no sign of cytotoxicity.[19−21]

Chart 1. Structures of Gd-DTPA-BMA and **6**

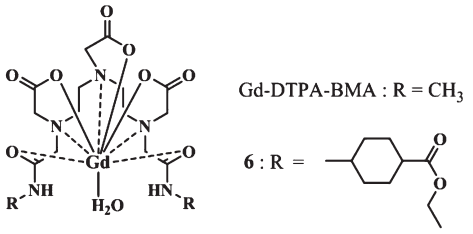

Herein, we report the design and the synthesis of a series of DOTA conjugates (**4a**−**c**) and their Gd-complexes of the type $[Gd(L)(H_2O)]\cdot xH_2O$ (**5a**−**c**, L = **4a**−**c**) for use as a new class of bifunctional MRI CAs with liver-specific and blood-pool properties.

Results and Discussion

Synthesis and Characterization. Scheme 1 shows the preparative method leading to the formation of DOTA conjugates of tranexamic acid (**4a**), tranexamic esters (**4b**,**c**), and their Gd(III) complexes (**5a**−**c**). The synthesis of **4** initially requires the formation of the hydrogen chloride salt of *trans*-4(aminomethyl)cyclohexanecarboxylic acid and its esters (**1a**−**c**) according to the literature method.[14,22] A simple reflux of **1** with bromoacetyl bromide in $CHCl_3$ resulted in corresponding amides (**2**) which were further reacted with DO3A-(^{t}BuO)$_3$ to give **3**. Subsequent deprotection of *tert*-butyl groups in **3** by trifluoroacetic acid (TFA) in the presence of NaOH resulted in the desired DO3A conjugates **4a**−**c**. They form Gd(III) complexes of the type [Gd(**4**)-$(H_2O)]\cdot xH_2O$ (**5**) by simple complexation with an equimolar amount of gadolinium chloride in water. All complexes were isolated as white, hygroscopic solids by repeated precipitation with cold diethyl ether from the reaction mixture.

The formation of **4** and **5** was confirmed by microanalysis and spectroscopic techniques such as ^{1}H and ^{13}C NMR and HRFAB- and MALDI-TOF mass spectrometry. IR spectroscopy is also informative in that the presence of carbonyl groups can be confirmed by a pair of intense carbonyl stretching bands assignable to the amide carbonyl (NHC═O) and carboxylic carbonyl (C═O) groups in the range 1602−1672 cm^{-1}.[23]

Protonation Constants and Stability Constants. Protonation constants (K_i^H) of **4** and stability constants of **5** are defined in eqs 1 and 2, respectively, where H_iL (L = **4**; i = 1, 2, ...) is the protonated ligand, L the totally deprotonated

Scheme 1. Synthesis of DOTA Conjugates of Tranexamic Acid (**4a**), Tranexamic Esters (**4b**,**c**), and Their Gd(III) Complexes (**5a**−**c**)

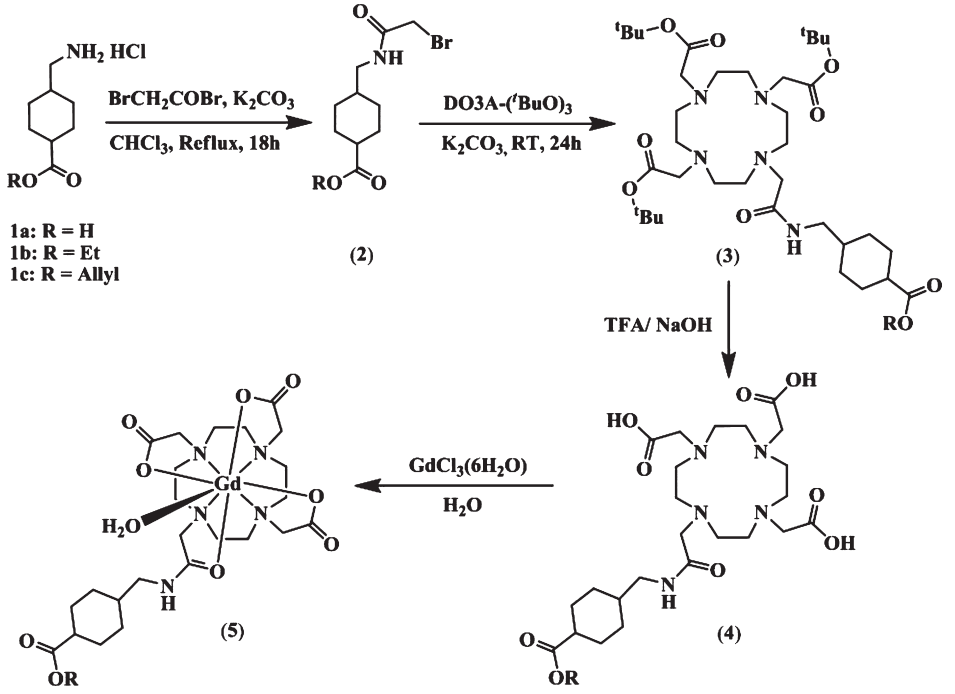

Table 1. Protonation Constants ($\log K_i^H$) of **4a**−**c** (I = 0.10 mol/dm^3)

	log K (25 °C, μ = 0.10 M (KCl))							
equilibrium	**4a**	**4b**	**4c**	DOTA[a]	DTPA[b]	EOB-DTPA[c]	BOPTA[d]	DTPA-BMA[e]
[HL]/[L][H]	11.73	10.80	10.62	12.09	10.49	10.91	10.71	9.37
[H_2L]/[HL][H]	8.91	9.35	8.64	9.68	8.60	8.63	8.21	4.38
[H_3L]/[H_2L][H]	4.93	5.24	5.45	4.55	4.28	4.26	4.35	3.31
[H_4L]/[H_3L][H]	4.87			4.13	2.64	2.73	2.83	
$\sum pK_a$	30.43	25.39	25.72	30.45	26.01	26.53	26.10	17.06

[a] Data obtained from ref 25. [b] Data obtained from ref 29. [c] Data obtained from ref 18. [d] Data obtained from ref 17. [e] Data obtained from ref 27.

Table 2. Stability (K_{ML}) and Selectivity Constants (K_{Sel}) of Gd-Complexes of **4a**−**c** (I = 0.10 mol/dm^3) and the pM[a] Values of the Complexes of Gd(III), Zn(II), Ca(II), and Cu(II) at pH 7.4

	log K (25 °C, μ = 0.10 M (KCl))							
equilibrium	**4a**	**4b**	**4c**	DOTA[b]	DTPA[c]	EOB-DTPA[d]	BOPTA[e]	DTPA-BMA[f]
[GdL]/[Gd][L]	24.58	22.07	21.52	25.30	22.46	23.46	22.6	16.85
{log $K_{GdL(pH7.4)}$}	18.73	16.72	16.99	18.33	18.14	18.7	18.4	14.84
[CaL]/[Ca][L]	14.01	15.42	14.97	17.23	10.75	11.74		7.17
{log $K_{CaL(pH7.4)}$}	8.16	10.06	10.44	10.26	6.43			5.11
[ZnL]/[Zn][L]	16.71	16.65	17.61	21.05	18.70			12.04
{log $K_{ZnL(pH7.4)}$}	10.86	11.29	13.08	14.08	14.38		13.9	10.02
[CuL]/[Cu][L]	17.56	17.39	19.30	22.63	21.38			13.03
{log $K_{CuL(pH7.4)}$}$_{7.4)}$	11.70	12.04	14.77	15.66	17.06		17.3	11.06
[log K_{sel}(Gd/Ca)]	10.56	6.65	6.55	8.07	11.71			9.68
[log K_{sel}(Gd/Zn)]	7.87	5.43	3.91	4.25	3.76			4.81
[log K_{sel}(Gd/Cu)]	7.02	4.68	2.21	2.67	1.08			3.82
pGd	17.73	15.72	15.99	19.2	17.14			13.88
pCa	7.16	9.06	9.43	-	5.45			4.19
pZn	9.86	10.29	12.08	15.19	13.39			9.06
pCu	10.70	11.04	13.77	14.05	16.06			10.05

[a] pM = $-\log[M^{n+}]_{free}$ at pH 7.4; $[M^{n+}]_{total}$ = 1 μmol/dm^3; $[L]_{total}$ = 1.1 μmol/dm^3. [b] Data obtained from refs 25 and 26. [c] Data obtained from ref 29. [d] Data obtained from ref 18 and 24. [e] Data obtained from ref 24. [f] Data obtained from ref 27.

free ligand, M the unhydrolyzed aquametal ion, and ML the nonprotonated and unhydrolyzed complex.

$$K_i^H = \frac{[H_iL]}{[H_{i-1}L][H^+]} \quad (1)$$

$$K_{ML(therm)} = \frac{[ML]}{[M][L]} \quad (2)$$

The protonation constants of **4a**−**c** and the stability constants of their Gd(III), Ca(II), Zn(II), and Cu(II) complexes were determined by potentiometric titration, and relevant data are collected in Table 1 along with those for DOTA and acyclic analogues such as DTPA and DTPA-BMA for comparative purposes. Table 1 shows that the present ligand series **4a**−**c** mostly exhibit protonation constants ($\log K_i^H$) and the overall basicity ($\sum pK_a$) values that are comparable with or slightly higher than those for their acyclic, open-chain counterparts. The overall basicity is directly correlated with the intensity of electrostatic interactions between the metal and the donor atoms of the ligand and thus with the stability of the chelate.

Higher basicity of the ligand will surely lead to the formation of a thermodynamically more stable complex, which is demonstrated with Gd-complexes of **4a**−**c** (entry 1, Table 2). In addition, two additional factors must have caused a further increase in the complex stability. They are (1) the macrocyclic effect and (2) the number of five-membered rings (N−Gd−N and N−Gd−O) formed by the chelate between the metal and the various donor atoms of the ligand.[24−26]

Table 2 shows the stability and selectivity constants of Gd-complexes **5a**−**c** and the pM values. When a comparison is made within the series, **4a** shows the highest values. In fact, the complex stability of GdL at physiological conditions becomes even greater than that of parent DOTA. Note that $\log K_{GdL}$ (pH 7.4) for **4a** is 18.73 while that for DOTA is 18.33 (cf. entry 2, Table 2). The highest complex stability achieved with **4a** may be explained in terms of a stronger electrostatic interaction with the Gd(III) ion compared with **4b** and **4c**, with $L^{4-} \leftrightarrow Gd^{3+}$ and $L^{3-} \leftrightarrow Gd^{3+}$, respectively.

The thermodynamic stability constant alone may not be sufficient to account for the stability of the complexes under physiological conditions.[26,27] The conditional stability constant or more frequently the pM value describes the stability of complexes under physiologically relevant conditions.[28] The pM value reflects the influence of ligand basicity and protonation of the complex. Thus, the larger the pM value, the higher is the affinity of the ligand for the metal ion under the given condition.[30] Table 2 shows that **4a**−**c** exhibit higher pM values with Gd(III) than with Ca(II), Zn(II), or Cu(II), indicating that the Gd(III) complexes of **4a**−**c** are stable enough to avoid any interference by other endogenous metal ions.

Transmetalation Kinetics. Gd-chelates, although they are thermodynamically stable, may be kinetically labile enough to undergo transmetalation by endogenous ions. In such a process, the paramagnetic Gd(III) ion is expelled from the complex. Endogenous ions likely to compete with Gd(III) are Cu(II), Ca(II), and Zn(II).[31−33] The Cu(II) ion is present in very small concentrations in the blood (1−10 μmol/L), whereas Ca(II) has relatively low affinity for acyclic ligands such as DTPA and DTPA-BMA (roughly 10 orders of magnitude lower than that of Gd(III)). Although the affinity for Ca(II) by cyclic ligand such as DOTA may be high enough

(cf. entry 3, Table 2), transmetalation by this ion can be ignored in the presence of other metal ions. For instance, only Zn(II) can displace a significant amount of Gd(III) because the concentration of the former in blood is relatively high (55−125 μmol/L), and its association constant toward DTPA and DOTA is only about 4 orders of magnitude lower than that of Gd(III) (cf. Table 2).[34] The stability of Gd-complexes in the presence of Zn(II) is thus an important issue because, as mentioned above, transmetalation will induce a release of Gd(III) into the body and possible depletion of the endogenous ion subsequent to its elimination as a hydrophilic complex by the kidneys.

If transmetalation of a soluble, paramagnetic gadolinium complex by diamagnetic Zn(II) ions were to occur in a phosphate-buffered solution, then the released Gd(III) would react to form $Gd_2(PO_4)_3$, the solubility of which is very low

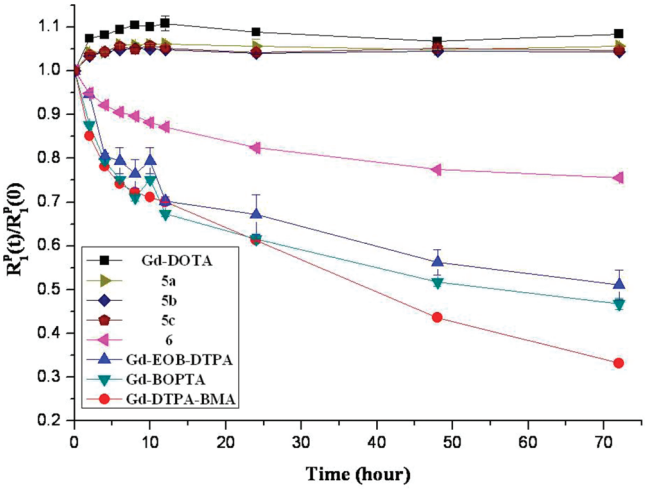

Figure 1. Evolution of $R_1^P(t)/R_1^P(0)$ as a function of time for various MRI CAs.

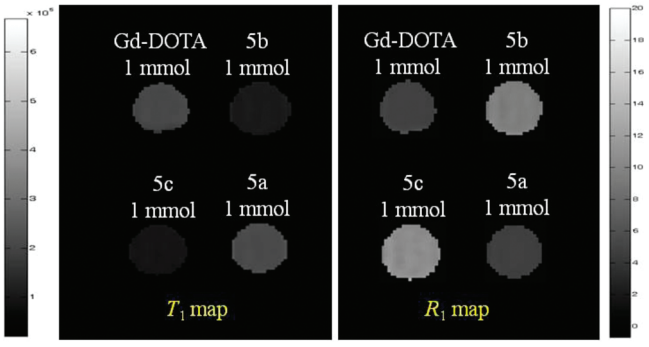

Figure 2. T_1 and R_1 maps on **5a**−**c** and Gd-DOTA.

(K_{sp} = $10^{-22.2}$ mol^2/L^2) and whose influence on the longitudinal relaxation rate of water is negligible.[35]

The relative value of R_1^P at any time t, $R_1^P(t)/R_1^P(0)$, is therefore a good estimate of the extent of transmetalation. Its evolution over time gives relevant information about the kinetics of the reaction, whereas the plateau value theoretically reached at $t = \infty$ will reflect the thermodynamic aspects of the system.

Figure 1 shows the evolution of the normalized paramagnetic longitudinal relaxation rates $R_1^P(t)/R_1^P(0)$ observed with the present series **5a**−**c**. For comparative purposes, the measurements were also made with Gd-DOTA, Gd-BOPTA, Gd-EOB-DTPA, Gd-DTPA-BMA, and other structurally related Gd-DTPA-bis(amide) conjugates of ethyl tranexamate (**6**). It is quite interesting to observe that all complexes put into test are grouped into two depending on the pattern of evolution: (1) those adopting macrocyclic chelates such as Gd-DOTA and **5a**−**c**; (2) those with acyclic chelates such as Gd-EOB-DTPA, Gd-BOPTA, Gd-DTPA-BMA, and **6**.

The most characteristic feature of **5a**−**c** is that they all possess pretty high kinetic stability (inertness) to retain more than 98% of the paramagnetic relaxation rate during the initial measurement for 72 h. They exhibit nearly the same behavior as Gd-DOTA. These observations may be as expected judging from their structural similarity, that is, the same number of five-membered chelates and the same macrocyclic motifs. The initial increases in the relaxation rate during the first 5 min found with **5** and Gd-DOTA may be due to the transient and better accessibility of gadolinium to water during the decomplexation process.[34,36,37]

On the other hand, those belonging to the second group exhibit a drastic decrease in the rate, which is expected judging from the fact that both adopt the acyclic, open-chain DTPA-bis(amide) motif. The slope becomes even steeper with Gd-DTPA-BMA to retain only 30% of the initial relaxation rate during the same period of measurement.

Here, an additional interesting point can be made concerning the plot observed with **6**. Namely, the plot is located approximately midway between plots for two groups. This observation suggests that the tranexamic moiety in DTPA-bis(amide) in **6** should play a key role in not only thermodynamic stability but also transmetalation kinetics. In this connection, it has already been pointed out that the presence of the tranexamic moiety helps to enhance R_1-relaxivity of **6** mostly through an increase in the rotational correlation time (τ_R) compared with simple DTPA-BMA.[13−15]

Relaxivity. Figure 2 shows the relaxation time (T_1) and relaxivity (R_1) maps on **5a**−**c** and Gd-DOTA. The phantom images were obtained with 1 mM solutions of complexes and with the same concentration of Gd-DOTA for comparative purposes. Table 3 summarizes the relaxation times (T_1 and T_2)

Table 3. T_1, R_1, T_2, and R_2 Values for **5a**−**c** and Clinically Used MRI CAs[a]

sample	T_1 (ms)	R_1 (mM^{-1} s^{-1})	T_2 (ms)	R_2 (mM^{-1} s^{-1})
5a	256.43 ± 2.63	3.9 ± 0.04	250.02 ± 2.50	4.0 ± 0.04
5b	116.29 ± 1.35	8.6 ± 0.10	108.75 ± 2.60	9.2 ± 0.22
5c	105.28 ± 1.33	9.5 ± 0.12	91.74 ± 0.25	10.9 ± 0.03
Gd-EOB-DTPA[b]	213.15 ± 9.07	4.7 ± 0.2	198.83 ± 23.4	5.1 ± 0.6
Gd-BOPTA[b]	250.62 ± 12.5	4.0 ± 0.2	235 ± 27.4	4.3 ± 0.5
Gd-DOTA	270.30 ± 2.92	3.7 ± 0.04	244.54 ± 12.5	4.1 ± 0.21
Gd-DTPA-BMA[c]	209.8 ± 5.82	4.9 ± 0.14	290.9 ± 21.02	3.4 ± 0.25
water[c]	842.5 ± 46.38	1.1 ± 0.06	1220 ± 167.20	0.82 ± 0.12

[a] Data presented as mean values ± SD. [b] Date obtained from ref 47. [c] Data obtained from ref 14.

and relaxivities (R_1 and R_2) for **5a**−**c** along with other Gd-complexes.

The most significant feature of Table 3 is that **5b** and **5c** exhibit significantly higher R_1 values than any of the clinically used MRI CAs, the highest R_1 reaching with **5c** up to 2.6 times as high as that of Gd-DOTA. Parallel observations in the R_1 increase have also been made earlier by us with **6**, Gd-complexes of DTPA-(bisamide) conjugates of tranexamates.[14,15] Although one might speculate a certain role played by tranexamate in the R_1 increase, a precise mechanism has yet to be clarified. Exceptionally low R_1 value with **5a** compared to the rest in the same series (cf. entry 1, Table 3) has to be clarified as well. A possible explanation may be given in connection with the presence of hydrophilic carboxylic acid (−COOH) in **5a**. This group would form hydrogen bonding with the inner-sphere water, thereby retarding the water-exchange rate (k_{ex}).[38]

In Vivo MRI Test. The in vivo MRI test was performed with **5c** along with those for liver-specific MRI CAs such as Gd-EOB-DTPA and Gd-BOPTA for comparative purposes.[16,39−42] Figure 3 shows the coronal T_1-weighted images of 6-week male Institute of Cancer Research (ICR) mice for **5c**. The most characteristic feature of **5c**, compared with Gd-BOPTA and Gd-EOB-DTPA, is that it shows a strong signal enhancement not only in liver but also in the heart and carotid artery (see Figure S1 for additional blood-pool enhancement at aorta). In line with this observation is the contrast-to-noise ratio (CNR) curve with **5c** to maintain the initial values as long as 1 h, as seen from Figure 5. Figure S1 is also supportive of this observation showing approximately 25% Gd-content in blood at 1 h after injection.

All three CAs show the excretion via bile duct, confirming hepatobiliary uptake as seen in Figure 4. Yet the tissue deposition is the lowest with **5c** (∼1%) (cf. Figure S2 and Table S1). Biliary and renal excretions with Gd-EOB-DTPA are reported to be 50% each, while biliary excretion reaches only 2−4% with Gd-BOPTA with renal excretion being predominant (75−99%).[43,44]

The indication is that **5c** resembles Gd-BOPTA in many respects. A minor difference has yet to be recognized in that the blood-pool enhancement lasts longer with **5c** than with Gd-BOPTA. Although such contrast enhancement not only in liver but in the blood as observed with **5c** is not without precedent, the most striking difference with **5c** and its predecessors may be explained in terms of the structural uniqueness of **5c**. Namely, the present system, unlike its predecessors, adopts macrocyclic chelate DOTA instead of acyclic DTPA and more importantly makes no resort to the presence of aromatic substituent(s) in the chelate backbone. The observance of the blood-pool enhancement by aromatic group(s) is considered to be the result of the lipophilic interaction with organs or blood cells. In this regard, both Gd-BOPTA and Gd-EOB-DTPA adopt acyclic DTPA moieties whose backbones are derivatized by aromatic residues in the expectation that their presence would increase noncovalent lipophilic interaction of MRI CA with organs or blood cells. Our findings with **5c**, therefore, seem to indicate that the presence of aromatics may not be an essential prerequisite for such a noncovalent lipophilic interaction of MRI CA with organs or blood cells.

Figure 5 shows the CNR profiles,[45,46] which are in accordance with the observations made in connection with Figures 3 and 4. Namely, strong and long enhancement for hepatocellular uptake is observed because of slow excretion through bile duct. The reason for slow excretion may be explained in terms of longer circulation time as demonstrated from the blood-pool effect. Increased lipophilicity of **5c** due to the presence of tranexamic unit might have caused such a blood-pool effect.

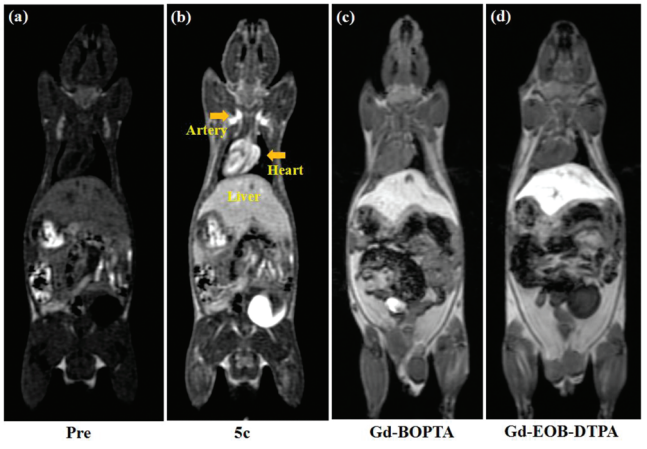

Figure 3. Coronal T_1-weighted whole body images of 6-week male ICR mice: (a) before injection; 10 min after injection with (b) **5c**, (c) Gd-BOPTA, and (d) Gd-EOB-DTPA at a dosage of 0.1 mmol/kg.

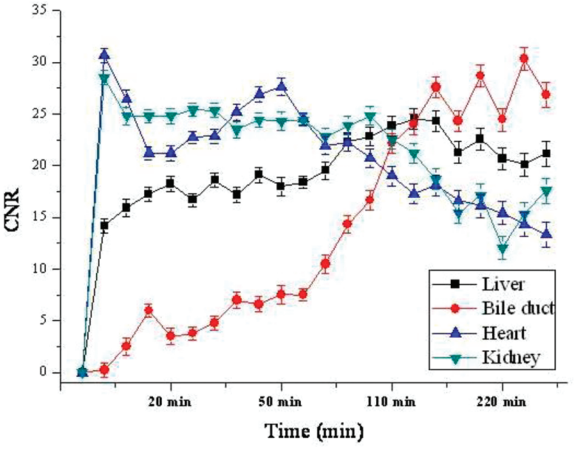

Figure 5. CNR profiles obtained by **5c** for liver, bile duct, heart, and kidney.

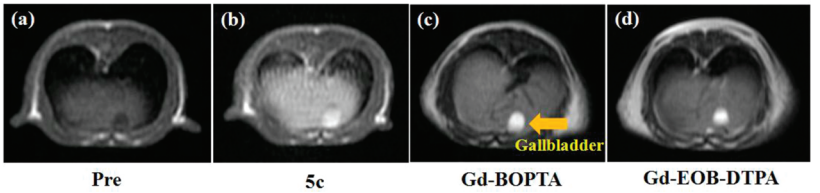

Figure 4. Axial T_1-weighted images for liver and gallbladder of 6-week male ICR mice before injection (a), 300 min after injection with **5c** (b), and 60 min after injection with Gd-BOPTA (c) and Gd-EOB-DTPA (d) at a dosage of 0.1 mmol/kg.

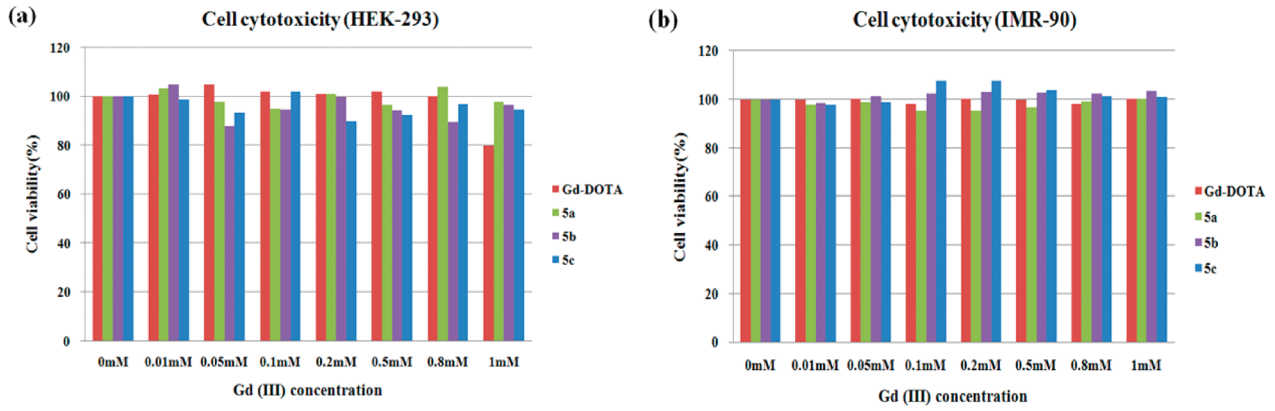

Figure 6. Relative cell cytotoxicity (%) of (a) the human embrionic kidney cells (HEK-293) and (b) human embryonic lung fibroblasts (IMR-90) obtained by Gd-DOTA and **5a**−**c**. The standard deviations (±SD) were obtained on a triplicate analysis (n = 3).

In Vitro Cell Cytotoxicity. The cytotoxicity tests were performed on human cell lines HEK-293 and IMR-90 with **5a**−**c**. Figure 6 demonstrates that the cell proliferation and the viability are not affected when incubated for 24 h. No obvious change is observed when a comparison is made of the cells' cytotoxicity assessment with the contrast agents. These observations indicate that the present series **5a**−**c** have very little or negligible cytotoxicity in the concentration range required for obtaining intensity enhancement in the MR images.

Conclusions

We have synthesized and successfully demonstrated that Gd-DOTA conjugates of tranexamic esters (**5**) can be a new class of MRI BPCAs with simultaneous contrast enhancement in liver. The structural uniqueness of **5** lies in the fact that, unlike their predecessors such as Gd-BOPTA and Gd-EOB-DTPA, they adopt macrocyclic DOTA instead of acyclic DTPA as ligand and that they carry no aromatic substituent(s) in the ligand backbone. R_1-relaxivities of **5b** and **5c** are higher than those of any of current MRI CAs, and their thermodynamic stabilities and kinetic inertness are comparable with or better than those of most of the current ECF and liver-specific MRI CAs. What is demonstrated by the presence of tranexamate is that it plays a key role in many respects such as an increase in R_1-relaxivity, an increase in thermodynamic stability as well as kinetic inertness, and blood-pool enhancement through noncovalent aliphatic interactions with organs or blood cells. In every respect, the present series may put an entry into a new family of practical MRI BPCAs with more merits than their predecessors.

Experimental Section

General Remarks. All reactions were carried out under an atmosphere of dinitrogen using the standard Schlenk techniques. Solvents were purified and dried using standard procedures. 1,4,7,10-Tetraazacyclododecane (DOTA) was purchased from Strem (U.S.) and *trans*-4-(aminomethyl)cyclohexanecarboxylic acid (tranexamic acid) was obtained from TCI (Japan) and used without further purification. All other commercial reagents were purchased from Aldrich and used as received unless otherwise stated. Deionized water was used for all experiments. The ^{1}H and ^{13}C NMR experiments were performed on a Bruker Advance 400 or 500 spectrometer at KBSI. Chemical shifts were given as δ values with reference to tetramethylsilane (TMS) as an internal standard. Coupling constants are in Hz. FAB mass spectra were obtained by using a JMS-700 model (Jeol, Japan) mass spectrophotometer. IR spectra were run on a Mattson FT-IR Galaxy 6030E spectrophotometer at KBSI. Elemental analyses were performed by Center for Scientific Instruments, KNU. The compounds **1b**,**c** were prepared according to the literature methods.[14,22] The purity of all products except **3b**, **3c**, and **4a** was determined with purity above 95% by elemental analysis. The purity of **5a**−**c** was double-checked by analytical and semipreparative reversed-phase HPLC with a UV−vis detection probing at 210 nm (KNAUER, VYDAC C-18 column with gradient elution using the mobile phases (A) H_2O containing 0.1% CF_3COOH and (B) MeCN containing 0.1% CF_3COOH).

Potentiometric Measurements and Computational Method. Potentiometric titrations were performed with an automatic titrator to determine the protonation constants of the DO3A conjugates of tranexamates and the stability constants of corresponding metal complexes. The autotitrating system consists of a 798 MPT titroprocessor, a 728 stirrer, and a PT-100 combination pH electrode (Metrohm). The pH electrode was calibrated using standard buffer solutions. All calibrations and titrations were carried out under a CO_2-free nitrogen atmosphere in a sealed glass vessel (50 cm^3) thermostated at 25 ± 0.1 °C at an ionic strength of 0.10 mol/dm^3 KCl. The concentrations of the metal ion and the amide solutions were maintained at approximately 0.5 mmol/dm^3. A CO_2-free KOH solution (0.100 mol/dm^3) was used as a titrant to minimize the changes in ionic strength during the titration. Dioxygen and carbon dioxide were excluded from the reaction mixtures by maintaining a positive pressure of purified nitrogen in the titration cell. The electromotive force of the cell is given by $E = E' + Q \log [H^+] + E_j$, and both $E'°$ and Q were determined by titrating a solution with a known hydrogen-ion concentration at the same ionic strength, using the acid range of the titration. The liquid-junction potential (E_j) was found to be negligible under the experimental conditions employed. The protonation constants of the ligands and the overall stability constants of various metal complexes formed in aqueous solutions were determined from the titration data using the computer program HYPERQUAD. The accuracy of this method was verified by measuring the protonation and the stability constants for Ca(II), Zn(II), Cu(II), and Gd(III) complexes of [DTPA-BMA]$^{3-}$. The results were compared with literature values.[27]

Transmetalation Kinetics. This experiment was prepared according to the literature method.[34] It is based on measurement of the evolution of the water proton longitudinal relaxation rate (R_1^P) of a buffered solution (phosphate buffer, pH 7.4) containing 2.5 mmol/L gadolinium complex and 2.5 mmol/L $ZnCl_2$. Then 10 μL of a 250 mmol/L solution of $ZnCl_2$ is added to 1 mL of a buffered solution of the paramagnetic complex. The mixture is vigorously stirred, and 300 μL is taken up for the relaxometric study. A control study, run on Gd-DTPA-BMA

and Gd-DOTA with zinc acetate, has given results identical to those obtained in the presence of $ZnCl_2$. The R_1^P relaxation rate is obtained after subtraction of the diamagnetic contribution of the proton water relaxation from the observed relaxation rate $R_1 = (1/T_1)$. The measurements were performed on a 3 T whole body system (Magnetom Tim Trio, Simens, Korea Institute of Radiological & Medical Science), at room temperature.

Synthesis. 2b. To a mixture of *trans*-4-(aminomethyl) cyclohexane ethyl carboxylate hydrochloride (3.00 g, 13.5 mmol) and K_2CO_3 (3.73 g, 27.1 mmol) in CH_3CN (100 mL) at 0 °C was added a solution of bromoacetyl bromide (1.1 mol equiv in 20 mL of CH_3CN) slowly over 1 h. After 18 h of stirring at 80 °C, the inorganic salts were removed by filtration and the organic phase was evaporated under reduced pressure. The residue was dissolved in CH_2Cl_2 and washed with H_2O (30 mL × 3 times). The organic phase was dried over Na_2SO_4, filtered, and evaporated to give a crude product which was further purified by chromatography on silica [gradient elution CH_2Cl_2 to 30% ethyl acetate (EA)-CH_2Cl_2, R_f = 0.5 (EA/CH_2Cl_2 = 4:6)] to obtain a white solid. Yield: 2.49 g (60%). ^{1}H NMR ($CDCl_3$): δ = 6.54 (br, 1H, −CONH−), 4.12 (q, 2H, $-OCH_2CH_3$), 3.90 (s, 2H, $BrCH_2CO-$), 3.16 (t, 2H, $-CONHCH_2-$), 2.22 (m, 1H, $CH_3CH_2COOCH-$, cyclohexyl), 1.80−2.10 (m, 4H, CH_2-, cyclohexyl), 1.52 (m, 1H, $NHCH_2CH-$, cyclohexyl), 1.49−1.37 (m, 2H, $-CH_2-$, cyclohexyl), 1.24 (t, 3H, $-COOCH_2CH_3$), 1.08−0.92 (m, 2H, $-CH_2-$, cyclohexyl). ^{13}C NMR ($CDCl_3$): δ = 175.79 ($BrCH_2CONH-$), 165.57 ($-COOCH_2CH_3$), 60.23 ($-COOCH_2CH_3$), 45.96 ($-COOCH-$, cyclohexyl), 43.17 ($-NHCH_2CH-$), 37.12($-NHCH_2CH-$, cyclohexyl), 29.68 ($BrCH_2CO-$), 29.35 ($-CH_2-$, cyclohexyl), 28.34 ($-CH_2-$, cyclohexyl), 14.22 ($-COOCH_2CH_3$). Anal. Calcd for $C_{12}H_{20}BrNO_3$: C, 47.07; H 6.58; N, 4.57. Found: C, 47.78; H, 6.85; N 4.72. FAB-MS (*m*/*z*): calcd for $C_{12}H_{21}BrNO_3$, 306.07 ($[MH]^+$). Found: 306.20.

2c. The title compound was prepared by following the same procedure described for **2b** by replacing ethyl-*trans*-4(aminomethyl) cyclohexanecarboxylate hydrochlride with ally-*trans*-4-(aminomethyl) cyclohexanecarboxylate hydrochloride (3.0 g, 12.83 mmol). The product was obtained as a white solid. Yield: 2.86 g (70%). ^{1}H NMR ($CDCl_3$): δ = 6.54 (br, 1H, −CONH−), 5.87−5.92 (m, 1H, $-OCH_2CH=CH_2$), 5.24−5.32 (m, 2H, $-OCH_2CH=CH_2$), 4.57 (d, 2H, $-OCH_2CH=CH_2$), 3.89 (s, 2H, $BrCH_2CONH-$), 3.16 (t, 2H, $-CH_2NHCO-$), 2.27 (m, 1H, $CH_2=CHCH_2COOCH-$), 1.82−2.03 (m, 4H, $-CH_2-$, cyclohexyl), 1.52 (m, 1H, $-NHCH_2CH-$), 1.46−1.51 (m, 2H, CH_2-, cyclohexyl), 0.92−1.10 (m, 2H, $-CH_2-$, cyclohexyl). ^{13}C NMR (DMSO-d_6): δ = 175.32 ($BrCH_2CONH-$), 165.33 ($-COOCH_2CH=CH_2$), 132.29 ($-COOCH_2CH=CH_2$), 118.01 ($-COOCH_2CH=CH_2$), 64.92 ($-COOCH_2CH=CH_2$), 45.98 ($-COOCH-$, cyclohexyl), 43.17 ($-NHCH_2CH-$), 37.12-($-NHCH_2CH-$, cyclohexyl), 29.68 ($BrCH_2CO-$), 29.44 ($-CH_2-$, cyclohexyl), 28.35 ($-CH_2-$, cyclohexyl). Anal. Calcd for $C_{13}H_{20}BrNO_3$: C, 49.07; H, 6.34; N, 4.40. Found: C, 48.90; H, 6.39; N, 4.27. FAB-MS (*m*/*z*): calcd For $C_{13}H_{21}BrNO_3$, 318.07 ($[MH]^+$). Found: 318.30.

DO3A-(^{t}BuO)$_3$·HBr. To a stirring mixture of cyclen (5.34 g, 30 mmol) and $NaHCO_3$ (8.34 g, 99 mmol) in CH_3CN (120 mL) at 0 °C was added dropwise *tert*-butyl bromoacetate (19.35 g, 99 mmol) dropwise over 30 min. The reaction mixture was further stirred for 48 h at room temperature. Any inorganic solids were removed by filtration, and the solvent was removed from the filtrate to leave a beige solid. The solid was taken up in chloroform, and the solid suspension was removed by filtration. The filtrate was concentrated, and the resulting solid recrystallized from toluene to afford the title compound as a white solid. Yield: 11.30 g (61%). ^{1}H NMR ($CDCl_3$): δ = 3.37 (s, 4H, 2 × CH_2 acetates), 3.29 (s, 2H, CH_2 unique acetate), 3.10 (br, 4H, $-CH_2CH_2-$ ring), 2.88−2.93 (br m, 12H, $-CH_2CH_2-$ ring), 1.55 (s, 27H, $-C(CH_3)_3$). ^{13}C NMR($CDCl_3$): δ = 28.19 (−C-(CH_3)), 47.52 ($-CH_2CH_2-$, cyclic ring, asymmetric), 49.15 ($-CH_2CH_2-$, cyclic ring, asymmetric), 51.31 ($-CH_2CH_2-$, cyclic ring, symmetric), 58.17 ($-CH_2COO-$, acetate), 81.66 ($-C(CH_3)$), 169.62 ($-CH_2COO-$, unique acetate), 170.51 ($-CH_2COO-$, acetate). Anal. Calcd for $C_{26}H_{51}N_4O_6$·HBr: C, 52.43; H, 8.63; N, 9.41. Found: C, 52.10; H, 8.90; N, 9.00. MALDI-TOF MS (*m*/*z*): calcd for $C_{26}H_{51}N_4O_6$, 515.38 ($[MH]^+$). Found: 515.39.

3b. To a stirred solution of **2b** (1.13 g, 3.69 mmol) in CH_3CN (10 mL) was added slowly a mixture of DO3A-(^{t}BuO)$_3$·HBr (2 g, 3.36 mmoL) and K_2CO_3 (1.40 g, 11.07 mmol) suspended in CH_3CN (50 mL). The mixture was stirred at room temperature for 24 h, after which any solids were removed by filtration. The filtrate was evaporated under a reduced pressure to yield a yellowish white solid. The crude compound was purified by chromatography on silica (gradient elution CH_2Cl_2 to 10% MeOH−CH_2Cl_2, R_f = 0.5 (MeOH/CH_2Cl_2 = 1:9)) to give a white solid. Yield: 2.11 g (85%). ^{1}H NMR ($CDCl_3$): δ = 4.11 (q, 2H, $-COOCH_2CH_3$), 3.38 (s, 4H, 2 × CH_2 acetate), 3.29 (s, 2H, CH_2 unique acetate), 3.05−3.15 (br m, 6H, overapped $-CH_2CH_2-$ ring and CH_2 acetate arm), 2.85−2.94 (br m, 12H, $-CH_2CH_2-$ ring), 2.18−2.24 (m, 1H, $CH_3CH_2COOCH-$), 1.88−2.00 (m, 4H, $-CH_2-$, cyclohexyl), 1.60 (m, 1H, $-NHCH_2CH-$, cyclohexyl), 1.46 (s, 27H, $-C(CH_3)_3$), 1.41−1.45 (m, 2H, $-CH_2-$, cyclohexyl), 1.25 (t, 3H, $-OCH_2CH_3$), 1.01−1.05 (m, 2H, $-CH_2-$,cyclohexyl). Anal. Calcd for $C_{39}H_{69}N_5O_9$: C, 62.29; H, 9.25; N, 9.31. Found: C, 53.73; H, 8.33; N, 7.90 (purity < 95%). FAB-MS (*m*/*z*): calcd for $C_{38}H_{70}N_5O_9$, 740.52 ($[MH]^+$); $C_{38}H_{69}N_5O_9Na$, 762.50 ($[MNa]^+$). Found: 740.40 ($[MH]^+$), 762.40 ($[MNa]^+$). MALDI-TOF MS (*m*/*z*): found, 740.50 ($[MH]^+$), 762.50 ($[MNa]^+$). The product was used without further purification for the synthesis of **4b**.

3c. The title compound was prepared by the same procedure for **3b** by replacing **2b** with **2c**. The product was obtained as a white solid. Yield: 2.10 g (83%). ^{1}H NMR ($CDCl_3$): δ = 5.85−5.95 (m, 1H, $-CH_2CH=CH_2$), 5.19−5.31 (m, 2H, $-CH_2CH=CH_2$), 4.54 (d, 2H, $-CH_2CH=CH_2$), 0.95−1.05 (m, 2H, $-CH_2-$, cyclohexyl), 1.37−1.45 (m, 2H, $-CH_2-$, cyclohexyl), 1.46 (s, 27H, $-C(CH_3)_3$), 2.21−3.51 (br m, 27H, overapped $-CH_2CH_2-$ cyclic ring (16H), $-CH_2-$ acetate arms (8H), $-NHCH_2CH-$ (2H), $-NHCH_2CH-$ (1H)), 1.90−2.00 (br m, 4H, $-CH_2-$, cyclohexyl), 1.60 (m, 1H, $-OOCCH_2CH-$). Anal. Calcd for $C_{39}H_{69}N_5O_9$: C, 62.29; H, 9.25; N, 9.31. Found: C, 54.42; H, 8.20; N, 7.86 (purity < 95%). MALDI-TOF MS (*m*/*z*) calcd for $C_{39}H_{69}N_5O_9Na$: 774.50 ($[MNa]^+$). $C_{39}H_{69}N_5O_9K$: 790.47 ($[MK]^+$). Found: 774.58 $[MNa]^+$, 790.60 $[MK]^+$. The product was used without further purification for the synthesis of **4b**.

4a. To a solution of **4b** (1.00 g, 1.00 mmol) in EtOH (20 mL) was added 5 N NaOH until the pH rose to 10. The solvent was then removed under a reduced pressure and the resulting residue taken up in methanol (10 mL). The solution was passed through a short column of silica gel (60 mesh) with methanol as an eluent. The residue obtained after removal of the solvent was triturated with diethyl ether and dried in vacuo to leave a white solid. Yield: 0.50 g (85%). ^{1}H NMR (D_2O): δ = 0.85−0.94 (m, 2H, $-CH_2-$, cyclohexyl), 1.20−1.29 (m, 2H, $-CH_2-$, cyclohexyl), 1.41 (br s, 1H, $-NHCH_2CH-$, cyclohexyl), 1.68−1.71 (m, 2H, $-CH_2-$, cyclohexyl), 1.80−1.83 (m, 2H, $-CH_2-$, cyclohexyl), 1.98−2.04 (m, 1H, $HOOCCH-$, cyclohexyl), 2.35−3.45 (br m, 26H, overapped $-CH_2CH_2-$ cyclic ring (16H), $-CH_2-$ acetate arms (8H), $-CONHCH_2-$(2H). ^{13}C NMR (D_2O): δ = 29.02 ($-CH_2CH_2-$, cyclohexyl), 29.74 ($-CH_2CH_2-$, cyclohexyl), 37.10 ($-(CH_2)_2CHCH_2NH-$, cyclohexyl), 44.80 ($-(CH_2)_2-CHCH_2NH-$), 45.63 ($-(CH_2)_2CHCOOH$), 48.67 ($-CH_2CH_2-$, cyclic ring, symmetric), 51.56 ($-CH_2CH_2-$, cyclic ring, asymmetric), 52.06 ($-CH_2CH_2-$, cyclic ring, asymmetric), 55.51 ($-CH_2COONH-$), 55.80 ($-CH_2COOH$, unique acetate), 57.12 ($-CH_2COOH$, acetates), 170.84 ($-CH_2CONH-$), 171.92 ($-CH_2COOH$, unique), 177.02 ($-CH_2COOH$), 183.70 ($-(CH_2)_2-CHCOOH$). Anal. Calcd for $C_{24}H_{41}N_5O_9$·3CF_3COOH: C, 40.68; H, 5.01; N, 7.91. Found: C, 36.23; H, 5.93; N, 7.37

(purity <95%). MALDI-TOF MS (*m*/*z*): calcd for $C_{24}H_{42}N_5O_9$, 544.30 ($[MH]^+$), $C_{24}H_{41}N_5O_9Na$, 566.28 ($[MNa]^+$) ; found, 544.35 ($[MH]^+$), 566.33 ($[MNa]^+$). The product was used without further purification for the synthesis of **5a**.

4b. A solution of **3b** (2.00 g, 2.70 mmol) in TFA (15 mL) was stirred at room temperature for 24 h. The solution was then diluted with diethyl ether (50 mL) to precipitate a white solid which was isolated by filtration, washed several times with diethyl ether, and dried under vacuum. The product was obtained as **4b**·3CF_3COOH as determined by acidimetric titration and by elemental analysis. The presence of CF_3COOH in the final product as an adduct was unavoidable, and parallel observations have also been made in the previous literature.[48] Yield: 2.25 g (91%). ^{1}H NMR (D_2O): δ = 3.95−4.01 (q, 2H, $-OCH_2CH_3$), 3.62 (br s, 8H, acetate arm $-CH_2-$), 3.14 (br s, 16H, $-CH_2CH_2-$ cyclic ring), 2.90−2.92 (d, 2H, $-CONHCH_2-$), 2.13−2.20 (m, 1H, $CH_3CH_2COOCH-$), 1.79−1.82 (m, 2H, $-CH_2-$, cyclohexyl), 1.62−1.65 (m, 2H, $-CH_2-$, cyclohexyl), 1.31−1.35 (m, 1H, $-NHCH_2CH-$, cyclohexyl), 1.19−1.27 (m, 2H, $-CH_2-$, cyclohexyl), 1.06−1.10 (t, 3H, $-OCH_2CH_3$), 0.79−0.89 (m, 2H, $-CH_2-$, cyclohexyl). ^{13}C NMR (500 NMR, D_2O): δ = 13.3 ($-CH_2CH_3$), 28.10 ($-CH_2CH_2-$, cyclohexyl), 29.10 ($-CH_2CH_2-$, cyclohexyl), 36.56 ($-(CH_2)_2CHCH_2NH-$, cyclohexyl), 43.16 ($-(CH_2)_2CHCH_2NH-$), 45.29 ($-(CH_2)_2CHCOOCH_2CH_3$), 49.12 ($-CH_2CH_2-$, cyclic ring, asymmetric), 50.25 ($-CH_2CH_2-$, cyclic ring, symmetric), 52.22 ($-CH_2COONH-$), 55.17 ($-CH_2COOH$, acetate), 171.01 ($-CH_2CONH-$), 179.32 ($-CH_2COOCH_2CH_3$), 181.36 ($-CH_2COOH$). Anal. Calcd for $C_{26}H_{45}N_5O_9$·3CF_3COOH: C, 42.06; H, 5.29; N, 7.66. Found: C, 42.09; H, 5.85; N, 8.26. MALDI-TOF-MS (*m*/*z*): calcd for $C_{26}H_{46}N_5O_9$, 572.33 ($[MH]^+$), $C_{26}H_{45}N_5O_9Na$, 594.31 ($[MNa]^+$). Found: 572.44 ($[MH]^+$), 594.44 ($[MNa]^+$).

4c. The title compound was obtained by following the same procedure as that for **4b** by replacing **3b** with **3c**. The product was obtained as a white solid. Yield: 2.60 g (89%). ^{1}H NMR (D_2O): δ = 5.84−5.94 (m, 1H, $-OCH_2CH=CH_2$), 5.18−5.28 (m, 2H, $-OCH_2CH=CH_2$), 4.53−4.55 (d, 2H, $-OCH_2CH=CH_2$), 3.61−3.72 (m, 8H, $-CH_2-$ acetate arms), 3.14−3.27 (br m, 16H, $-CH_2CH_2-$ cyclic ring), 2.98−2.99 (d, 2H, $-CONHCH_2-$), 2.27−2.34 (m, 1H, $CH_3CH_2COOCH-$, cyclohexyl), 1.91−1.93 (m, 2H, $-CH_2-$, cyclohexyl), 1.72−1.74 (m, 2H, $-CH_2-$, cyclohexyl), 1.40−1.48 (m, 1H, $-NHCH_2CH-$, cyclohexyl), 1.28−1.37 (m, 2H, $-CH_2-$, cyclohexyl), 0.88−0.98 (m, 2H, $-CH_2-$, cyclohexyl). ^{13}C NMR (500 NMR, D_2O): δ = 28.09 ($-CH_2CH_2-$, cyclohexyl), 29.05 ($-CH_2CH_2-$, cyclohexyl), 36.51 ($-(CH_2)_2CHCH_2NH-$, cyclohexyl), 43.06 ($-(CH_2)_2CHCH_2NH-$), 45.35 ($-(CH_2)_2CHCOOCH_2CH=CH_2$), 49.52 ($-CH_2CH_2-$, cyclic ring), 52.21 ($-CH_2COONH-$), 55.12 ($-CH_2COOH$, acetate), 65.58 ($-COOCH_2CH=CH_2$), 118.03 ($-COOCH_2CH=CH_2$), 132.06 ($-COOCH_2CH=CH_2$), 171.99 ($-CH_2CONH-$), 179.73 ($-CH_2COOCH_2CH=CH_2$), 181.28 ($-CH_2COOH$). Anal. Calcd for $C_{27}H_{45}N_5O_9$·2.4CF_3COOH: C, 43.76; H, 5.65; N, 8.28. Found: C, 43.65; H, 6.03; N, 9.07. MALDI-TOF MS (*m*/*z*): calcd for $C_{27}H_{46}N_5O_9$, 584.33 ($[MH]^+$), $C_{27}H_{45}N_5O_9Na$, 606.31 ($[MNa]^+$). Found: 584.36 ($[MH]^+$), 606.32 ($[MNa]^+$).

5a. To a solution of **4a** (0.5 g, 0.9 mmol) in deionized water (10 mL) was added gadolinium(III) chloride hexahydrate (0.34 g, 0.92 mmol), and the contents were stirred at room temperature for 18 h. The pH was periodically checked and adjusted to 7.0−8.0 using 1 N NaOH. After 18 h, the reaction mixture was passed through Sephadex G-25 to remove free Gd^{3+} ions from the product solution. The solution was dried under vacuo, and the remaining oily product was taken up in EtOH to which was added dropwise diethyl ether to precipitate the product. The white solid was removed by filtration, washed with diethyl ether, and dried under vacumn. The absence of free Gd^{3+} from the final product was checked with an orange indicator xylenol.[49] The product was obtained as a hygroscopic white solid. Yield 0.71 g (90%). Anal. Calcd for $NaC_{24}H_{40}GdN_5O_{10}$·3$H_2O$: C, 36.40; H, 5.73; N, 8.84. Found: C, 36.86; H, 4.97; N, 7.50. FAB-MS (*m*/*z*): calcd for $C_{24}H_{38}GdN_5O_9Na$, 721.18 ($[MNa - (H_2O)]^+$). Found: 721.19. HR-FABMS (*m*/*z*): calcd for $C_{24}H_{39}GdN_5O_9$, 699.1989 ($[MH - (H_2O)]^+$); found, 699.1984. HPLC (semipreparative, 4.6 mm × 250 mm, flow rate of 1 mL/min, retention time of 19.70 min)

5b. The title compound was obtained by following a similar procedure as that for **5a** by replacing **4a** with **4b** (0.913 g, 1 mmol). Yield: 1.12 g (95%). Anal. Calcd for $C_{26}H_{44}GdN_5O_{10}$·13H_2O: C, 31.93; H, 7.21; N, 7.16. Found: C, 31.51; H, 5.02; N, 6.01. HR-FABMS (*m*/*z*): calcd for $C_{26}H_{42}GdN_5O_9Na$, 749.2128 ($[MNa - (H_2O)]^+$). Found: 749.2126. HPLC (analytical, 2.1 mm × 250 mm, flow rate of 0.5 min/L, retention time of 9.90 min).

5c. The title compound was obtained essentially by adopting the same procedure as that for **5a** by replacing **4a** with **4c** (0.857 g, 1 mmol). Yield 1.01 g (90%). Anal. Calcd for $C_{27}H_{44}GdN_5O_{10}$·12H_2O: C, 33.36; H, 7.05; N, 7.20. Found: C, 32.69; H, 5.22; N, 6.70. HR-FABMs (*m*/*z*): calcd for $C_{27}H_{43}GdN_5O_9$, 739.2308 ($[MH - (H_2O)]^+$); found, 739.2307. HPLC (analytical, 2.1 mm × 250 mm, flow rate of 0.5 min/L, retention time of 20.90 min).

Relaxivity. T_1 measurements were carried out using an inversion recovery method with a variable inversion time (TI) at 1.5 T (64 MHz). The MR images were acquired at 35 different TI values ranging from 50 to 1750 ms. T_1 relaxation times were obtained from the nonlinear least-squares fit of the signal intensity measured at each TI value. For T_2 measurements the CPMG (Carr−Purcell−Meiboon−Gill) pulse sequence was adapted for multiple spin−echo measurements. Thirty-four images were acquired with 34 different echo time (TE) values ranging from 10 to 1900 ms. T_2 relaxation times were obtained from the nonlinear least-squares fit of the mean pixel values for the multiple spin−echo measurements at each echo time. Relaxivities (R_1 and R_2) were then calculated as an inverse of relaxation time per mM. The determined relaxation times (T_1 and T_2) and relaxivities (R_1 and R_2) are finally image-processed to give the relaxation time map and relaxivity map, respectively.

In Vitro Cell Cytotoxicity. IMR-90 (human embryonic lung fibroblasts) and HEK-293 (human embryonic kidney cells) were used. Cells were maintained in DMEM (Gibco) supplemented with heat-inactivated FCS (10%), penicillin (100 IU/mL), and streptomycin (100 mg/mL) (all purchased from Gibco). The medium was replaced every 2 days, and cells were split into a 96-well plate (IMR-90, 5×10^3 cells/well; HEK-293, 1×10^4 cells/well). Various **5a**−**c** concentrations (0.01−2.0 mM) of the contrast agent were added into the culture serum free media followed by incubation for 24 h. Then 10 μL of stock MTT solution (5 mg/mL, Sigma) was added to each well, and cells were incubated for 4 h at 37 °C in a 5% CO_2 environment. The medium was aspirated from the well without disturbing the formazan crystals. DMSO (100 μL) was added to each well. The plates were shaken for 5 min on a plate shaker, and the absorbance at 570 nm was measured by ELISA reader.[50,51]

In Vivo MR Experiments. The in vivo study was performed in accordance with the rules of the animal research committee of Kyungpook National University. Six-week male ICR mice with weights of 29−31 g were used for the in vivo study. The mice (n = 6) were anesthetized by 1.5% isoflurane in oxygen. Measurements were made before and after injection of **5c** via tail vein. The amount of CA per each injection is as follows: 0.1 mmol of Gd/kg for MR images. After each measurement the mouse was revived from anesthesia and placed in the cage with free access to food and water. During these measurements, the animals were maintained at approximately 37 °C using a warm water blanket.

MR images were taken with a 1.5 T MR unit (GE Healthcare, Milwaukee, WI) equipped with a homemade small animal rf coil. The coil was of the receiver type with its inner diameter

being 50 mm. The imaging parameters for 3D fast SPGR (spoiled GRASS images) are as follows: repetition time (TR) = 8.8 ms; echo time (TE) = 3.9 ms; 10 mm field of view (FOV); 256 × 192 matrix size; 1.0 mm slice thickness; number of acquisition (NEX) = 4. The imaging parameters for spin−echo are as follows: TR = 500 ms; TE = 13 ms; 6 mm FOV; 192 × 128 matrix size; 1.5 mm slice thickness; NEX = 4. Each image was taken at an interval of 3 min and 16 s. MR images were obtained for 26 h after injection.

The anatomical locations with enhanced contrast were identified with respect to liver, bile duct, heart, and kidney on postcontrast MR images. For quantitative measurement, signal intensities in specific regions of interest (ROI) were measured using Advantage Window software (GE Medical, U.S.). The CNR was calculated using eq 3, where SNR is the signal-to-noise ratio.

$$\mathrm{CNR} = \mathrm{SNR}_{\mathrm{post}} - \mathrm{SNR}_{\mathrm{pre}} \quad (3)$$

Biodistribution Studies. 5c was administered intravenously as a bolus (0.1 mmol/kg) in a tail vein of 25 male mice (ICR, 30−35 g). The mice were anesthetized and killed by means of exsanguination from the vena cava at each time point (after 1, 6, 24, 48, and 72 h injection time). The gadolinium concentration was measured in tissues (liver, kidneys, bile duct, blood, and intestine). The gadolinium concentration was determined by digesting the tissues with HNO_3 (65%) at 180 °C for 120 min and measuring the concentration in the clear diluted solution by inductively coupled plasma atomic emission spectrometry (ICP-AES, Optima 7300DV, PerkinElmer, U.S.). Detection limit of this method is 0.01 ppm.[52]

Acknowledgment. Financial support from NRF (Grant No. 2009-0088454), NRF (Grant No. 2009-0072413), and The Advanced Medical Technology Cluster for Diagnosis & Prediction, Kyungpook National University, Korea, from MKE, ROK (Grant No. RTI04-01-01) is gratefully acknowledged. Drs. Keongmin Kim and Ji-Ae Park are greatly appreciated for their assistance in the kinetic studies.

Supporting Information Available: Blood-pool effect and biodistribution data for **5c**. This material is available free of charge via the Internet at http://pubs.acs.org.

References

(1) Caravan, P. Strategies for increasing the sensitivity of gadolinium based MRI contrast agents. *Chem. Soc. Rev.* **2006**, *35* (6), 512–523.
(2) Caravan, P.; Ellison, J. J.; McMurry, T. J.; Lauffer, R. B. Gadolinium(III) chelates as MRI contrast agents: structure, dynamics, and applications. *Chem. Rev.* **1999**, *99* (9), 2293–2352.
(3) Penfield, J. G.; Reilly, R. F. What nephrologists need to know about gadolinium. *Nat. Clin. Pract. Nephrol.* **2007**, *3* (12), 654–668.
(4) Frullano, L.; Rohovec, J.; Peters, J. A.; Geraldes, C. F. G. C. Structures of MRI contrast agents in solution. *Top. Curr. Chem.* **2002**, *221*, 25–60.
(5) Raymond, K. N.; Pierre, V. C. Next generation, high relaxivity gadolinium MRI agents. *Bioconjugate Chem.* **2005**, *16* (1), 3–8.
(6) Datta, A.; Raymond, K. N. Gd-hydroxypyridinone (HOPO)-based high-relaxivity magnetic resonance imaging (MRI) contrast agents. *Acc. Chem. Res.* **2009**, *42* (7), 938–947.
(7) Hermann, P.; Kotek, J.; Kubicek, V.; Lukes, I. Gadolinium(III) complexes as MRI contrast agents: ligand design and properties of the complexes. *Dalton Trans.* **2008**, 3027–3047.
(8) Merbach, A. E.; Tóth, É. *The Chemistry of Contrast Agents in Medical Magnetic Resonance Imaging*; Wiley-VCH: Chichester, U.K., 2001.
(9) Bellin, M.-F. MR contrast agents, the old and the new. *Eur. J. Radiol.* **2006**, *60* (3), 314–323.
(10) Jacques, V.; Desreux, J. F. New classes of MRI contrast agents. *Top. Curr. Chem.* **2002**, *221*, 123–164.
(11) Clarkson, R. B. Blood-pool MRI contrast agents: properties and characterization. *Top. Curr. Chem.* **2002**, *221*, 201–235.
(12) Que, E. L.; Chang, C. J. Responsive magnetic resonance imaging contrast agents as chemical sensors for metals in biology and medicine. *Chem. Soc. Rev.* **2010**, *39* (1), 51–60.
(13) Kim, H.-K.; Lee, G.-H.; Kim, T.-J.; Chang, Y. Determination of correlation times of new paramagnetic gadolinium MR contrast agents by EPR and O-17 NMR. *Bull. Korean Chem. Soc.* **2009**, *30* (4), 849–852.
(14) Dutta, S.; Park, J. A.; Jung, J. C.; Chang, Y.; Kim, T. J. Gd-complexes of DTPA-bis(amide) conjugates of tranexamic acid and its esters with high relaxivity and stability for magnetic resonance imaging. *Dalton Trans.* **2008**, *16*, 2199–2206.
(15) Dutta, S.; Kim, S.-K.; Patel, D. B.; Kim, T.-J.; Chang, Y. Some new DTPA-*N*,*N*′-bis(amides) functionalized by alkyl carboxylates: synthesis, complexation and stability properties. *Polyhedron* **2007**, *26*, 3799–3809.
(16) Geraldes, C. F. G. C.; Laurent, S. Classification and basic properties of contrast agents for magnetic resonance imaging. *Contrast Media Mol. Imaging* **2009**, *4* (1), 1–23.
(17) Uggeri, F.; Aime, S.; Anelli, P. L.; Botta, M.; Brocchetta, M.; de Haeen, C.; Ermondi, G.; Grandi, M.; Paoli, P. Novel contrast agents for magnetic resonance imaging. Synthesis and characterization of the ligand BOPTA and its Ln(III) complexes {Ln = Gd, La, Lu}. *Inorg. Chem.* **1995**, *34* (3), 633–642.
(18) Schmitt-Willich, H.; Brehm, M.; Ewers, C. L.; Michl, G.; Muller-Fahrnow, A.; Petrov, O.; Platzek, J.; Raduchel, B.; Sulzle, D. Synthesis and physicochemical characterization of a new gadolinium chelate: the liver-specific magnetic resonance imaging contrast agent Gd-EOB-DTPA. *Inorg. Chem.* **1999**, *38* (6), 1134–1144.
(19) Svahn, C. M.; Merenyi, F.; Karlson, L.; Widlund, L.; Gralls, M. Tranexamic acid derivatives with enhanced absorption. *J. Med. Chem.* **1986**, *29* (4), 448–453.
(20) Katsuta, Y.; Yoshida, Y.; Kawai, E.; Suetsugu, M.; Kohno, Y.; Inomata, S.; Kitamura, K. *trans*-4-(Aminomethyl) cyclohexane carboxylic acid methylamideinhibits the physical interaction between urokinase-type plasminogen activator and stratum corneum, and accelerates the recovery of barrier function. *J. Dermatol. Sci.* **2005**, *40* (3), 218–220.
(21) Guo, J.-P.; Liu, B.-P.; Lv, X.-C.; Tan, Z.-C.; Tong, B.; Shi, Q.; Wang, D.-F. Molar heat capacities, thermodynamic properties, and thermal stability of *trans*-4-(aminomethyl)cyclohexanecarboxylic acid. *J. Chem. Eng. Data* **2007**, *52* (5), 1678–1680.
(22) Dutta, S.; Kim, S.-K.; Lee, E. J.; Kim, T.-J.; Kang, D.-S.; Chang, Y.; Kang, S. O.; Han, W.-S. Synthesis and magnetic relaxation properties of paramagnetic Gd-complexes of new DTPA-bis-amides. The X-ray crystal structure of $[Gd(L)(H_2O)]\cdot 3H_2O$ (L = DTPA-bis(4-carboxylicphenyl)amide). *Bull. Korean Chem. Soc.* **2006**, *27* (7), 1038–1042.
(23) Eckelman, W. C.; Karesh, S. M.; Reba, R. C. New compounds: fatty acid and long chain hydrocarbon derivatives containing a strong chelating agent. *J. Pharm. Sci.* **1975**, *64* (4), 704–706.
(24) Port, M.; Idee, J. M.; Medina, C.; Robic, C.; Sabatou, M.; Corot, C. Efficiency, thermodynamic and kinetic stability of marketed gadolinium chelates and their possible clinical consequences: a critical review. *BioMetals* **2008**, *21* (4), 469–490.
(25) Kumar, K.; Chang, C. A.; Francesconi, L. C.; Dischino, D. D.; Malley, M. F.; Gougoutas, J. Z.; Tweedle, M. F. Synthesis, stability, and structure of gadolinium(III) and yttrium(III) macrocylcic poly(amino carboxylates). *Inorg. Chem.* **1994**, *33* (16), 3567–3575.
(26) Kumar, K.; Tweedle, M. F.; Malley, M. F.; Gougoutas, J. Z. Synthesis, stability, and crystal structure studies of some Ca^{2+}, Cu^{2+}, and Zn^{2+} complexes of macrocylcic polyamino carboxylates. *Inorg. Chem.* **1995**, *34* (26), 6472–6480.
(27) Cacheris, W. P.; Quay, S. C.; Rocklage, S. M. The relationship between thermodynamics and toxicity of gadolinium complexes. *Magn. Reson. Imaging* **1990**, *8* (4), 467–481.
(28) Laus, S.; Ruloff, R.; Toth, E.; Merbach, A. E. GdIII complexes with fast water exchange and high thermodynamic stability: potential building blocks for high-relaxivity MRI contrast agents. *Chem.—A Eur. J.* **2003**, *9* (15), 3555–3566.
(29) Martell, A. E.; Smith, R. M. *Critical Stability Constants*; Plenum: New York, 1974; Vol. 1.
(30) Bannochie, C. J.; Martell, A. E. Synthesis, separation, and equilibrium characterization of racemic and meso forms a new multidentate ligand: *N*,*N*′-trimethylenebis[2-(2-hydroxy-3,5-dimethylphenyl)-glycine], TMPHPG. *Inorg. Chem.* **1991**, *30* (6), 1385–1392.
(31) Puttagunta, N. R.; Gibby, W. A.; Puttagunta, V. L. Comparative transmetallation kinetics and thermodynamic stability of gadolinium-DTPA bis-glucosamide and other magnetic resonance imaging contrast media. *Invest. Radiol.* **1996**, *31* (10), 619–624.
(32) Corot, C.; Idee, J. M.; Hentsch, A. M.; Santus, R.; Mallet, C.; Goulas, V.; Bonnemain, B.; Meyer, D. Structure−activity relationship

of macrocyclic and linear gadolinium chelates: investigation of transmetallation effect on the zinc-dependent metallopeptidase angiotension-converting enzyme. *J. Magn. Reson. Imaging* **1998**, *8* (3), 695–702.
(33) Corot, C.; Hentsch, A.-M.; Curtelin, L. Interaction of gadolinium complexes with metal-dependent biological systems. *Invest. Radiol.* **1994**, *29* (Suppl. 2), S164–S167.
(34) Laurent, S.; Vander Elst, L.; Copoix, F.; Muller, R. N. Stability of MRI paramagnetic contrast media: a proton relaxometric protocol for transmetallation assessment. *Invest. Radiol.* **2001**, *36* (2), 115–122.
(35) Laurent, S.; Vander Elst, L.; Muller, R. N. Comparative study of the physicochemical properties of six clinical low molecular weight gadolinium contrast agents. *Contrast Media Mol. Imaging* **2006**, *1* (3), 128–137.
(36) Wedeking, P.; Kumar, K.; Tweedle, M. F. Dissociation of gadolinium chelates in mice: relationship to chemical characteristics. *Magn. Reson. Imaging* **1992**, *10* (4), 641–648.
(37) Laurent, S.; Parac-Vogt, T. N.; Kimpe, K.; Thirifays, C.; Binnemans, K.; Muller, R. N.; Vander Elst, L. Bis(phenylethylamide) derivatives of Gd-DTPA as potential receptor-specific MRI contrast agents. *Eur. J. Inorg. Chem.* **2007**, *14*, 2061–2067.
(38) Toth, E.; Helm, L.; Merbach, A. E. Relaxivity of MRI contrast agent. *Top. Curr. Chem.* **2002**, *221* (45), 62–98.
(39) Semelka, R. C.; Helmberger, T. K. Contrast agents for MR imaging of the liver. *Radiology* **2001**, *218* (1), 27–38.
(40) Karabulut, N.; Elmas, N. Contrast agents used in MR imaging of the liver. *Diagn. Interventional Radiol.* **2006**, *12* (1), 22–30.
(41) Kirchin, M. A.; Pirovano, G. P.; Spinazzi, A. Gadobenate dimeglumine (Gd-BOPTA). An overview. *Invest. Radiol.* **1998**, *33* (11), 798–809.
(42) Pediconi, F.; Fraioli, F.; Catalano, C.; Napoli, A.; Danti, M.; Francone, M.; Venditti, F.; Nardis, P.; Passariello, R. Gadobenate dimeglumine (Gd-DTPA) vs gadopentetate dimeglumine (Gd-BOPTA) for contrast-enhanced magnetic resonance angiography (MRA): improvement in intravascular signal intensity and contrast to noise ratio. *Radiol. Med.* **2003**, *106* (1−2), 87–93.
(43) Karabulut, N.; Elmas, N. Contrast agents used in MR imaging of the liver. *Diagn. Interventional Radiol.* **2006**, *12*, 22–30.
(44) Lee, N. K.; Kim, S.; Lee, J. W.; Lee, S. H.; Kang, D. H.; Kim, G. H.; Seo, H. I. Biliary MR imaging with Gd-EOB-DTPA and its clinical applications. *Radiographics* **2009**, *29*, 1707–1724.
(45) Kiryu, S.; Inoue, Y.; Watanabe, M.; Izawa, K.; Shimada, M.; Tojo, A.; Yoshikawa, K.; Ohtomo, K. Evaluation of gadoxetate disodium as a contrast agent for mouse liver imaging: comparison with gadobenate dimeglumine. *Magn. Reson. Imaging* **2009**, *27* (1), 101–107.
(46) Schima, W.; Petersein, J.; Hahn, P. F.; Harisinghani, M.; Halpern, E.; Saini, S. Contrast-enhanced MR imaging of the liver: comparison between Gd-BOPTA and Mangafodipir. *J. Magn. Reson. Imaging* **1997**, *7* (1), 130–135.
(47) Rohrer, M.; Bauer, H.; Mintorovitch, J.; Requardt, M.; Weinmann, H. J. Comparison of magnetic properties of MRI contrast media solutions at different magnetic field strengths. *Invest. Radiol.* **2005**, *40* (11), 715–724.
(48) Barge, A.; Tei, L.; Upadhyaya, D.; Fedeli, F.; Beltrami, L.; Stefania, R.; Aime, S.; Cravotto, G. Bifunctional ligands based on the DOTA-monoamide cage. *Org. Biomol. Chem.* **2008**, *6*, 1176–1184.
(49) Barge, A.; Cravotto, G.; Gianolio, E.; Fedeli, F. How to determine free Gd and free ligand in solution of Gd chelates. A technical note. *Contrast Media Mol. Imaging* **2006**, *1* (5), 184–188.
(50) Zou, C.; Shen, Z. An optimized in vitro assay for screening compounds that stimulate liver cell glucose utilization with low cytotoxicity. *J. Pharmacol. Toxicol. Methods* **2007**, *56* (1), 58–62.
(51) Huh, M.-I.; Lee, Y.-M.; Seo, S.-K.; Kang, B.-S.; Chang, Y.; Lee, Y.-S.; Fini, M. E.; Kang, S.-S.; Jung, J.-C. Roles of MMP/TIMP in regulating matrix swelling and cell migration during chick corneal development. *J. Cell. Biochem.* **2007**, *101* (5), 1222–1237.
(52) Lokling, K. E.; Fossheim, S. L.; Klaveness, J.; Skurtveit, R. Biodistribution of pH-responsive liposomes for MRI and a novel approach to improve the pH-responsiveness. *J. Controlled Release* **2004**, *98*, 87–95.